

Vibrational population dynamics of the Hgl photofragment in ethanol solution

Nick Pugliano, Arpad Z. Szarka, S. Gnanakaran, Matt Triechel, and Robin M. Hochstrasser

Citation: *The Journal of Chemical Physics* **103**, 6498 (1995); doi: 10.1063/1.470376

View online: <http://dx.doi.org/10.1063/1.470376>

View Table of Contents: <http://scitation.aip.org/content/aip/journal/jcp/103/15?ver=pdfcov>

Published by the [AIP Publishing](#)

Articles you may be interested in

[The short-time intramolecular dynamics of solutes in liquids. II. Vibrational population relaxation](#)

J. Chem. Phys. **107**, 3098 (1997); 10.1063/1.474664

[Vibrational relaxation of Hgl in ethanol: Equilibrium molecular dynamics simulations](#)

J. Chem. Phys. **105**, 3486 (1996); 10.1063/1.472218

[B→X transitions in HgCl and Hgl](#)

Appl. Phys. Lett. **41**, 789 (1982); 10.1063/1.93704

[HgBr and Hgl Bstate quenching rate constants](#)

Appl. Phys. Lett. **34**, 324 (1979); 10.1063/1.90791

[Reactions of Metal Atoms. III. The Combination of Mercury and Iodine Atoms and the Spectrum of Hgl](#)

J. Chem. Phys. **52**, 4569 (1970); 10.1063/1.1673687



Vibrational population dynamics of the HgI photofragment in ethanol solution

Nick Pugliano, Arpad Z. Szarka, S. Gnanakaran, Matt Triechel, and Robin M. Hochstrasser

Department of Chemistry, 231 South 34th Street, University of Pennsylvania, Philadelphia, Pennsylvania 19104

(Received 8 September 1994; accepted 14 July 1995)

The vibrational population dynamics of HgI fragments in ethanol solution, resulting from the 320 nm photolysis of HgI₂, are examined both experimentally and by a simulation. The experiments reveal an HgI population distribution which rapidly relaxes toward equilibrium. At the earliest times, the HgI exhibits vibrational coherent wave-packet motion that dephases with a time constant of ca. 1 ps. These data are used to gain insight into the character of the solvated potential energy curves. The population relaxation was adequately reproduced by master equations which were formulated to incorporate the HgI anharmonicity and a solvent frequency dependent friction. This treatment characterizes the spontaneous vibrational relaxation timescale for the $n''=1\rightarrow 0$ transition to be ca. 3 ps, and is used to identify the relaxation rate constants for all other HgI level pairs. The simulations estimate that the initial excess energy of HgI is centered at $n''\cong 10$ which corresponds to a total excess energy of ca. 1050 cm⁻¹. © 1995 American Institute of Physics.

I. INTRODUCTION

The relaxation of vibrational energy in diatomic molecules is a fundamental component of chemical reaction dynamics in solids,¹ liquids,² and solutions.³ In high pressure gases and liquids a basic question which remains unresolved, is the detailed manner by which a vibrationally hot diatomic molecule approaches equilibrium with its surroundings.⁴ Experimental studies of such relaxation can expose the influence of the external solvent forces acting on a single mode, free from the complications arising from internal mode coupling, such as occurs in polyatomic molecules.^{5,6} In liquids, experiments on highly excited diatomic molecules produced by photoreactions have begun to appear only recently⁷⁻¹⁰ and there is a need for more investigations of this type. In addition, computer simulations based on classical dynamics have been employed to predict the nature of the forces involved in such energy relaxation processes.¹¹⁻¹³ The appropriateness of such simulations in predicting the relaxation of quantum mechanical oscillators in model liquids is also being evaluated^{14,15} but methods for the prediction of these processes in real solutions need considerably more development.

Vibrationally hot diatomic molecules resulting from chemical reactions are readily generated and are often studied in gases.¹⁶ The timescales of the relaxation dynamics are controllable in such cases by changing the pressure of a buffer gas. Reactions having these characteristics form the basis of infrared chemical lasers.¹⁷ In solutions, the "collisional" frequency is in excess of 10¹³ s⁻¹ and the corresponding relaxation processes can be extremely fast if the solute-solvent forces are sufficiently large. Therefore, the study of vibrational relaxation of hot diatomics in solutions relies heavily on the recent developments of ultrafast laser methods. Three systems have been reported on recently. The most extensively studied is hot neutral I₂ (Ref. 7) which is created by solvent cage induced recombination of the photo-

dissociated atoms. Vibrationally hot I₂⁻ is obtained by photodissociating I₃⁻ in solution^{8,9} and hot HgI was detected following the photolysis of HgI₂.^{10,18,19} For the case of I₂, the relaxation dynamics depend greatly on the solvent. Timescales in different solvents have been reported and range from 50 to 200 ps.⁷ The hot ion I₂⁻ dissipates its energy on the timescale of a few ps in ethanol.^{8,9} The polar HgI also cools on the timescale of a few ps in ethanol.^{10,18,19} Each of these systems presents an opportunity to evaluate the effectiveness of different types of intermolecular forces related to vibrational relaxation. A systematic study of the mechanism of vibrational cooling in HgI has not previously been presented and forms the subject of this paper.

The photolysis of HgI₂ has been well characterized by a number of groups and the early work has been reviewed by Maya.²⁰ Excitation of gas phase HgI₂ into its lowest energy absorption band is known to produce ground state HgI free radicals with a quantum yield of unity.²⁰ The excitation of this HgI₂ absorption band results in a branching of the I atom photofragment between its ²P_{3/2} and ²P_{1/2} ground and excited spin-orbit components. The spin-orbit splitting is ca. 7600 cm⁻¹ and the pump wavelength dependence of the branching has been characterized in the gas phase by Hoffmann and Leone.²¹ Finally, the vibrational frequencies for HgI₂ corresponding to the symmetric stretch, the asymmetric stretch and the bend are 155, 237, and 33 cm⁻¹, respectively.²² The lowest energy absorption spectrum of HgI₂ in ethanol is very similar to that in the gas phase.²³

The $B\ ^2\Sigma^+ \rightarrow X\ ^2\Sigma^+$ emission of the HgI free radical has been carefully studied in the gas phase by a number of groups.²⁴⁻²⁷ These experiments have determined that the equilibrium bond length decreases substantially (which is typical for an ion pair \rightarrow valence transition) from 3.3 to 2.8 Å when the molecule electronically relaxes from the *B* to the *X* state. This is corroborated by the calculations of Wadt²⁸ which characterize the ionic character, and the dipole moments in these electronic states of the HgCl and HgBr radi-

icals. The extensive data set has provided an accurate determination of the potential energy surfaces for both the ground and excited states, the transition dipole moment function for the $B \leftrightarrow X$ transition²⁷ and the vibrational frequencies for the X and B states which are 125 and 110 cm⁻¹, respectively.

Ultrafast studies of HgI₂ dissociation by Zewail and co-workers,²⁹ have illustrated isolated molecule dynamics on the femtosecond timescale. These experiments demonstrated that a vibrational coherent superposition state of HgI was created by the reaction, and the wave packets were modeled using quantum propagation methods.³⁰ The transients also provided evidence for the branching between the spin-orbit states of atomic iodine and this has been further verified by femtosecond time-of-flight techniques.³¹ This work confirmed that the $^2P_{3/2}$ atomic I channel resulted in vibrationally hot HgI, whereas the $^2P_{1/2}$ channel produced relatively cold HgI product. The dissociation dynamics of highly excited states of HgI₂ have most recently been investigated by means of multiphoton absorption³² to characterize a number of dissociative pathways that lead to highly energetic products.

A study of the vibrational energy cooling of solvated HgI therefore presents an opportunity to evaluate a number of important parameters of relaxation dynamics for a reaction which has been well characterized in the gas phase. The present work is aimed at characterizing the dynamics of energy flow from HgI to ethanol solvent after the photodissociation of HgI₂. The HgI generated in the photoreaction is highly vibrationally excited. This permits an opportunity to explore solute-solvent interactions over much of the potential surface and thereby examine the effects of anharmonicity on vibrational energy relaxation. This system is particularly unique for a number of reasons. The fact that the dipole moment decreases as the HgI bond stretches is a novel characteristic which presents challenges to condensed phase theory. The lower energy potential surfaces of HgI are well known in the isolated molecule and this will allow an evaluation of the effective potential functions in solution. Furthermore, the similarity of the HgI vibrational frequency to those of I₂ and I₂⁻ should permit meaningful comparisons with these systems.

II. EXPERIMENT

The femtosecond spectrometer used to conduct these experiments is based on the 20 Hz Nd:YAG amplification of a CPM laser. The CPM is first preamplified in two stages up to an energy of ca. 10 μJ and the output is recompressed to ca. 100 fs with a grating pair. The light is variably attenuated and imaged into a short piece of optical fiber. The output of the fiber extends from 570 nm to beyond 700 nm. This beam is collimated and used to seed a three stage amplifier for which the medium is a mixture of DCM and Rhodamine 590 dye. After Nd:YAG amplification up to the 500 μJ level, the 40 nm wide spectral profile centered at 620 nm is double passed through a grating compressor and a prism compressor to achieve 20 fs pulses.³³ This beam is separated into two parts. One portion is frequency doubled in a 50 μm slice of BBO and the transmitted 320 nm beam is collimated and separated from the residual 620 nm light with reflective di-

electric mirrors. Deconvolution of the cross correlation of the 320 nm beam with the 20 fs 620 nm pulse results in a 35–40 fs UV pulsewidth. This represents more than a twofold increase in time resolution over the work presented in Ref. 10. The second portion of the 620 nm beam is variably delayed and focused into an ethylene glycol jet to generate a continuum and this provides tunability from ca. 400 nm into the near infrared. Spectral selection of a particular probe wavelength is accomplished with 10 nm wide interference filters. The probe is split into two equal portions which serve as a signal and reference beam, each of which is detected with photodiodes. The photodiode signals are processed with box-car integration and the results are stored in units of absorbance. Averaging ca. 2000–3000 laser shots permits a minimum detectable fractional absorbance change of ca. 5×10^{-4} .

The sample was a 0.5 mm flowing jet of an ethanol solution containing HgI₂ at a concentration of 10 mM. The HgI₂ (99.999% purity Aldrich) was used as received, without further purification. For this HgI₂ concentration, only 60% of the pump light was absorbed. UV pump energies were always maintained at ca. 2 μJ. Under these conditions, saturation effects were not observed and all signals linearly followed the pump intensity. Time zero was found by conducting a pump-probe experiment on a molecule such as a stilbene. The estimated uncertainty in t_0 is no larger than ca. ±20 fs. The delay line was scanned linearly from -1 to +1 ps with 50 fs steps and logarithmically thereafter.

III. RESULTS AND ASSIGNMENTS

The lowest energy absorption band of HgI₂ in ethanol peaks at 273 nm and apart from the spectral maximum shifting approximately 1400 cm⁻¹ to lower energy relative to the gas phase absorption band, the shape is essentially unchanged.^{23,34} Therefore, the shapes of the HgI₂ surfaces in the Franck-Condon region and the initial internal dynamics along the dissociative coordinate are probably similar to those for the isolated molecule. Furthermore, the primary photoproducts should be HgI and I ($^2P_{3/2}$) when the solvated molecule is photolyzed at 320 nm. The time and frequency resolved data support this expectation.

A. Gas phase potential surfaces

The gas phase potentials are well characterized from the results of $B \rightarrow X$ emission experiments.^{24–27} For simplicity the ground and excited state potential surfaces were fit to Morse functions of the form,

$$U(r) = T_e + D_0 [1 - \exp(-\beta(r - r_e)/r_e)]^2 \quad (1a)$$

and the X state vibrational energies are described by

$$\frac{E_n''}{hc} = \omega_e \left(n + \frac{1}{2} \right) - x_e \omega_e \left(n + \frac{1}{2} \right)^2 \quad (1b)$$

The parameters for the HgI $X \ ^2\Sigma^+ / B \ ^2\Sigma^+$ states in Eq. (1a) are $T_e = 0/24\ 072 \text{ cm}^{-1}$, $D_0 = 2800/18\ 850 \text{ cm}^{-1}$, $\beta = 7.1/2.86$, and $r_e = 2.8/3.3 \text{ \AA}$. These potentials are illustrated in Fig. 1 by the dashed curves. Open and solid arrows are used to depict transitions which originate from low and high energy regions of the X state, respectively. It is apparent from this drawing that higher frequency probes mainly sample the

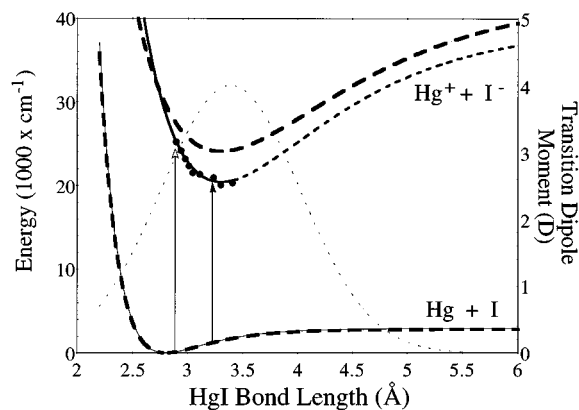


FIG. 1. The gas phase potentials for the $X\ 2\Sigma^+$ ground state and the $B\ 2\Sigma^+$ excited state of HgI are shown as heavily dashed lines. The $X\ 2\Sigma^+$ state dissociates to atoms whereas the $B\ 2\Sigma^+$ asymptotically approaches an ion pair. The equilibrium separation of the B state is shifted to 3.3 Å relative to that of the X state in which the minimum is 2.8 Å. The thin X state corresponds to the potential of mean force. The data points describe the experimentally determined portion of the effective B state as described in Sec. III E, and the line through the points is the best fit Morse potential. Only the solid portion of the line is determined by the analysis. The lightly dashed line is the transition dipole moment function of Ref. 27 used in the analysis.

bottom of the X -state potential, whereas lower frequency probes sample mainly the higher energy portions of the surface.

The observed energies for the vibrational eigenstates in the X state, agree well with those obtained from Eq. (1b), with $\omega_e = 125\text{ cm}^{-1}$ and $x_e\omega_e = 1.38\text{ cm}^{-1}$. The $B \leftrightarrow X$ transition dipole moment of Ref. 27 was used. Using this functional form for $\mu(r)$ an absorption spectrum for the $B \rightarrow X$ transition was calculated. Each vibrational wave function was calculated using a Numerov–Cooley algorithm³⁵ and the transition moment matrix elements, $\langle B_{n'} | \mu(r) | X_{n''} \rangle$ were determined over the range of excited and ground state vibrational levels from $200 < n' < 0$ and $42 < n'' < 0$, respectively. For these surfaces the transition matrix elements $\langle B_{n'} | \mu(r) | X_{n''} \rangle$ in the probe wavelength region used in our experiments have significant magnitude at HgI bond lengths corresponding to the attractive region of the X state and the repulsive region of the B state. The shapes of the potentials are expected to be least affected by solvent in the region probed because the B state is least polar there. In the B state, HgI asymptotically correlates to separated ions ($\text{Hg}^+ + \text{I}^-$) while it correlates to atoms in the X state. For simulations of the solution spectrum each vibronic transition was broadened by 80 cm^{-1} . This corresponds to an electronic dephasing time of at most 125 fs which is slightly faster than the dephasing time reported for I_2 .³⁶

B. Equilibrium simulations of the X surface

Molecular dynamics simulations of HgI in ethanol using Charmm³⁷ were used to calculate the potential of mean force for the HgI, X state. The dipole moment was first calculated for each internuclear separation by means of the *ab initio* effective core potentials^{38–40} as implemented in GAUSSIAN 92.⁴¹ With the dipole represented by point charges at the atomic centers, 50 ps simulations were run at ten internuclear

separations and the results used to calculate the solvent induced forces along the internuclear axis. These forces were then added to those known for isolated HgI to obtain a mean force potential. The convergence error was estimated⁴² to be $\pm 35\text{ cm}^{-1}$. This new surface was very similar to that of isolated HgI, and showed an increase in well depth of only 3%. These results tell us that if the nuclei of HgI were to move slowly enough in comparison to the energy changes resulting from solvent reorganization, the mean potential experienced would not be much altered from that of the isolated molecule. A less physically relevant limit is when the solvent response is very slow and there is no reorganization energy. In this case there will be an inhomogeneous distribution of surfaces governing the faster HgI motion. The mean well depth can be estimated from the simulation as the average of the solute–solvent interaction energy at the minimum compared with the separated atom configuration. For HgI(X) this energy was found to be 1800 cm^{-1} . At present the true situation is not known but these calculations suggest that the shape of the effective HgI potential will be a reasonable starting point for the analysis. The results presented in subsections D and E below further confirm the reasonableness of this assumption and at the same time permit a fuller characterization of a solvent perturbed surface. First, the nature of the signals observed in the experiments are described in subsection C.

C. The wavelength dependence of the probe signal

The population decay measurements reported below deal with time delays, τ , in excess of ca. 1 ps. It follows that the pump–probe signal can be calculated from a single time ordering of pump and probe fields corresponding to the case in which the pump fields are first absorbed followed by a coupling to the weak probe field. The probe signal, $S(\tau)$ measured under magic angle conditions, can be expressed by a first-order interaction of the evolving system with probe field:

$$S(\tau) = \text{Re} \frac{4\pi}{3\hbar c_0} \left\{ \sum_{n', n''} \omega |\mu_{n''n'}|^2 \int_{-\infty}^{\infty} dt \epsilon(t - \tau) \times \int_{-\infty}^t dt' \epsilon(t' - \tau) \rho_{n''}(t') \exp(\Omega_{n''n'}(t' - t)) \right\}. \quad (2)$$

In Eq. (2) $\epsilon(\tau)$ is the real probe pulse field envelope, $\mu_{n''n'}$ is the transition dipole connecting vibrational states $|X, n''\rangle$ and $|B, n'\rangle$, $\rho_{n''}(t)$ is the population of state n'' at time t , $\Omega_{n''n'} = i\Delta_{n''n'} + \Gamma_{n''n'}$ such that $\Delta_{n''n'} = \omega_{n''n'} + \omega_0$ with $\omega_{n''n'} = \omega_{n''} - \omega_{n'}$ being the transition angular frequency, $\Gamma_{n''n'}$ is the electronic dephasing for the $(B, n') \leftarrow (X, n'')$ transition and ω is the center frequency of the femtosecond probe. Equation (2) is the time domain version of the overlap of the pulse spectrum with the spectrum of the $B \leftarrow X$ transition of HgI. The integral over t accounts for the detector being too slow to follow the field envelope or the free induction decay of the sample. The detector integrates the square of the fields incident upon it.

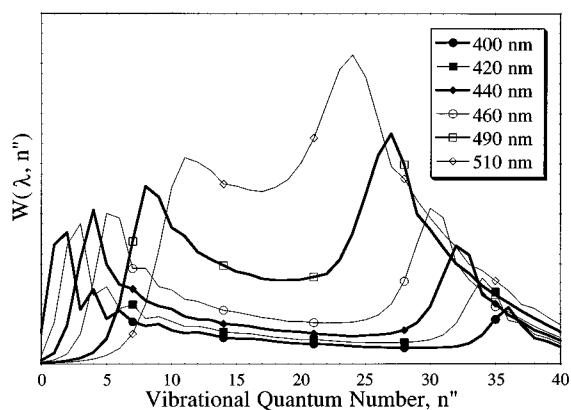


FIG. 2. Spectral window functions for each wavelength are plotted as a function of the HgI vibrational quantum number. The legend in the figure identifies each of the curves with respect to the center wavelength of the probe filter.

If the density matrix, $\rho_{n''}(t)$ describing the pure population dynamics is slowly varying compared to $\epsilon(t)$ and $(\Gamma_{n''n'})^{-1}$. Fourier transformation of the fields in Eq. (2) results in the following form of the HgI response to the femtosecond probe,

$S(\omega, \tau)$

$$= \text{Re} \frac{4\pi}{3\hbar c_0} \left\{ \omega \sum_{n', n''} \rho_{n''}(\tau) |\mu_{n''n'}|^2 \int_{-\infty}^{\infty} \frac{d\omega I(\omega)}{\Omega_{n''n'}(\omega)} \right\}. \quad (3)$$

In this equation $I(\omega)$ is the intensity spectrum of the probe pulse and the delay time τ is assumed to be larger than the probe pulse width. The form of $I(\omega)$ in our experiments is well represented by a Gaussian having a FWHM, σ , of 10 nm and a probe laser center frequency, ω obtained from the probe used. These parameters are the characteristics of the interference filters used in the wavelength selection scheme. It follows that the integrand in Eq. (3) can be rewritten as the product of a Gaussian with a complex Lorentzian ($1/\Omega_{n''n'}(\omega)$). Integration of this expression over all ω leads to the following computationally useful relationship,^{43(a)}

$$S(\omega, \tau) = \text{Re} \frac{4\pi}{3\hbar c_0} \omega \sum_{n', n''} \rho_{n''}(\tau) |\mu_{n''n'}|^2 \times \left\{ -i \sqrt{\frac{\pi}{2\sigma^2}} w \left(\frac{p_{n''n'}}{\sqrt{2}\sigma} \right) \right\} \quad (4)$$

in which w is the complex error function. Calculating the response simply thereby reduces to finding the single pole $p_{n''n'}$,⁴³ of the integrand in Eq. (4) and evaluating the real portion of the function. The response of the density matrix to the probe is dominated by the larger of the two spectral widths corresponding to the linewidth of the vibronic transition or the spectrum of the femtosecond probe pulse.

The Franck–Condon predictions pictorially represented in Fig. 2, can be quantitatively evaluated by calculating the contribution of absorption at each probe wavelength from each X-state vibrational level. This takes the form of a spec-

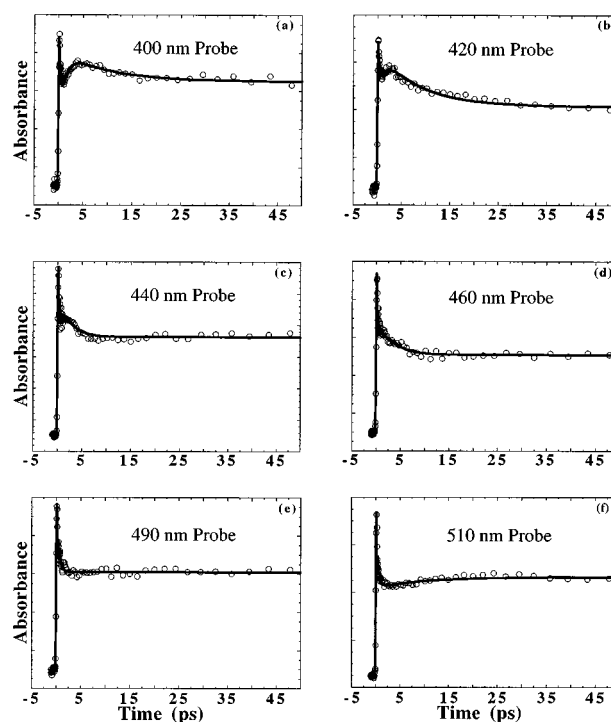


FIG. 3. The wavelength dependence of the transient absorptions resulting from the photolysis of a 10 mM solution of HgI₂ in ethanol with a 40 fs pulse centered at 320 nm. The solid lines represent multiexponential fits to the slowly varying parts data.

tral function and comes directly from Eq. (2). The spectral functions, or window functions,^{43(b)} $W(\omega, n'')$, defined through Eq. (2) as

$$S(\omega, \tau) = \sum_{n''} \rho_{n''}(\tau) W(\omega, n'') \quad (5)$$

are shown in Fig. 2 for an electronic dephasing rate $\Gamma_{el}=0.008 \text{ fs}^{-1}$. The plots in Fig. 2 provide a measure of the contribution to the absorption by a particular n'' for a given probe pulse defined by the spectral profile $I(\omega)$.

D. Population dynamics

The probe wavelength dependence of the transients is presented in Fig. 3. Each transient was fit to a multiexponential response function. The best fit parameters which characterize the data are listed in Table I. These results illustrate that the peak signals of these time-dependent features occur later as the probe is tuned to higher frequency. With the

TABLE I. Fitting parameters for the growth and decay portions of the population dynamics. The 490 and 510 nm data were fit only to decay terms.

	τ_{growth} (ps)	τ_{decay} (ps)
400 nm	0.95 (4)	10 (2)
420 nm	0.6 (1)	8.5 (5)
440 nm	0.8 (2)	3.2 (2)
460 nm	0.6 (2)	2.2 (8)
490 nm	...	0.49 (3)
510 nm	...	0.45 (3)

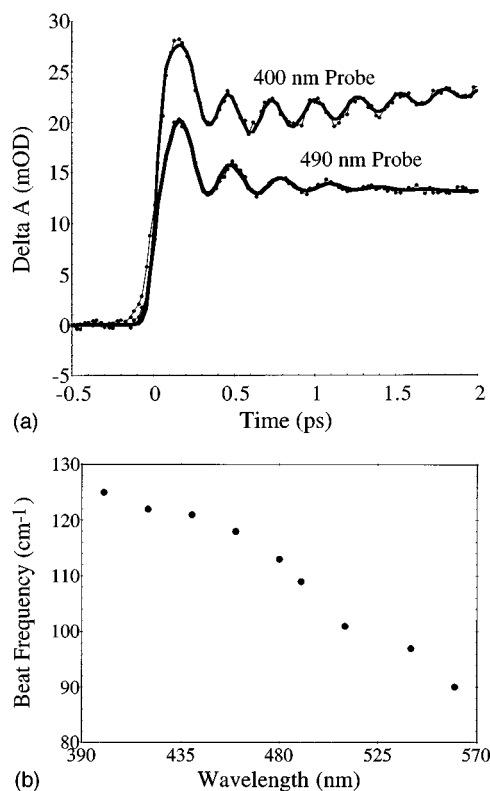


FIG. 4. (a) Typical transient responses recorded when probing a photolyzed sample of HgI₂ in ethanol. The oscillatory portion of the 400 and 490 nm data fit to frequency of 124.7 and 109 cm⁻¹, respectively. (b) The variation of the HgI oscillation frequency with the center wavelength of the relevant spectral (window) function.

exception of the data probed at 510 nm, each transient fully relaxes to an absorbance plateau which shows no subsequent temporal dependence on the picosecond timescale. A small component of the 510 nm transient grows slightly with a time constant of 9.7 ± 2 ps. This is suggested to be the time constant for a diffusion controlled bimolecular reaction between the photofragments and the solvent. These data form the subject of this paper, however to interpret them we required a more accurate assessment of the effective potential surface for the *X* state in the solvent and the Franck–Condon surface of the *B* state reached by optical transitions from *X*. For this purpose we now incorporate some relevant information on the vibrational quantum beats.

E. Estimates of the *X* and *B* surfaces in solution

In Fig. 4(a), femtosecond transients are shown for probe wavelengths of 400 and 490 nm. The higher time step density enables the oscillatory signal component to become clearly evident. A full characterization and analysis of the modulated signal component will be addressed in another manuscript,⁴⁴ but several points regarding these data are needed to validate the analysis of the slower time dynamics. The dephasing time of the vibrational wave packet is sufficiently fast (less than ca. 1 ps) so that the slower dynamics (Sec. III D) can be analyzed without consideration of the beats. In other words, the values of τ needed for evaluation of $\rho_{n''}(\tau)$ are in excess of the dephasing times of the vibra-

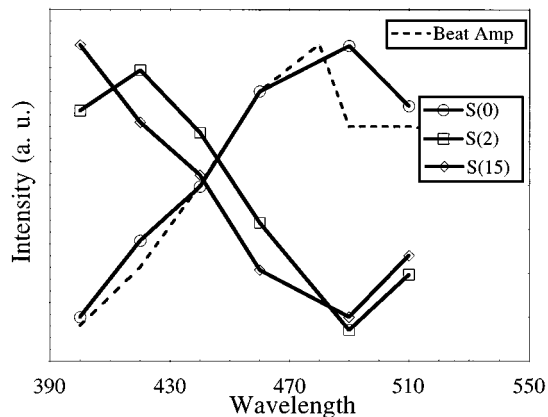


FIG. 5. Time-dependent absorption spectra are shown for HgI in ethanol following a 320 nm femtosecond excitation of HgI₂. The dashed line corresponds to the wavelength dependence of the amplitudes of the oscillatory components of the signals. Spectra are also presented from the fits of Fig. 3 and Table I. The zero time spectrum, $S(0)$ is extrapolated from the fits and is defined as $S(0)/S(\infty)$. The remaining two spectra are defined by the expression $\{S(t) - S(0)\}/S(\infty)$.

tional levels pairs in the HgI ground state potential surface. The oscillations in the 400 and 490 nm probe data fit to frequencies of 124.7 and 109.3 cm⁻¹, respectively. The analysis of the window functions between the shifted *X* and *B* states illustrated through Fig. 2 indicates that the 400 nm probe should primarily sample an energetically low lying portion of the HgI eigenstate distribution, which is confirmed by the fact that the observed frequency of 124.7 cm⁻¹ is close to the gas phase 0→1 frequency of 125 cm⁻¹. The 490 nm probe sets up a window between the *X* and *B* states which predominantly originates from high lying *n''* states. As expected, a lower frequency is observed consistent with the gas phase anharmonic potential.^{24–27} A complete set of the oscillation frequencies observed at various probe wavelengths is shown in Fig. 4(b). These data clearly show that the probe interrogates levels in the *X* state with frequencies between 90 and 125 cm⁻¹ over the wavelength region used. The 400 nm probe is initiating transitions from *close* to the bottom of the *X* potential. This is clear from the population dynamics (Fig. 3) which when probed at 400 nm show first a rise then a decay corresponding to population passing through the 400 nm spectral window.

The observation of oscillations represents the probing of a vibrational wave packet generated by the impulsive photodissociation of HgI₂. The beats fit to a phase of $\approx 0.9\pi$,^{10,18} which is consistent with the HgI bond being born initially compressed, and that the probe wavelengths couple the attractive side of the HgI *X* state with mainly the repulsive portion of the *B* state, as is expected from an analysis of the gas phase HgI potentials (see Fig. 1). More importantly, it verifies the presence of HgI in solution and that the potential surfaces are similar to those of the gas phase. An independent measure of the HgI spectrum at early times can be obtained from the contribution of the oscillatory component amplitude to the total signal at each probe wavelength. The spectrum of this amplitude vs wavelength is shown in Fig. 5. It peaks at ca. 480 nm, again consistent with expectations for hot HgI ($B^2\Sigma^+ \leftarrow X^2\Sigma^+$) based on calculations of the spec-

trum from gas phase potentials. Spectra were also generated from the wavelength dependence of the molecular response functions that characterize the slower dynamics represented in Fig. 5 and Table I. These are also plotted in Fig. 5 for pump–probe time delays of 0 (extrapolated), 2, and 15 ps. The zero time spectrum coincides well with the spectrum independently obtained from the amplitudes of the oscillations. The spectra at 2 and 15 ps show that the electronic spectrum shifts to higher energy as the pump–probe time delay is increased. This spectral evolution is indicative of the vibrational relaxation of HgI in solution, and is assigned as such. At a pump–probe time delay of 15 ps, the data of Fig. 3 reach a constant amplitude that can be used to estimate the static absorption spectrum of the molecular species present at that time. The spectra of Fig. 5 show that the HgI vibrationally hot spectrum cools to form the low energy side of its thermally equilibrated absorption spectrum.

Potentials for the X and B states of HgI that are consistent with all the data presented can be calculated on the assumption that the transition dipole function is unchanged in solution. The beat frequencies indicate which X -state level dominates the signal at each probe wavelength; the probe wavelength fixes the mean vertical energy separation between points on the X and B potentials; the observation of a phase shift of ca. π confirms that the points are on the repulsive wall of the X state. The resulting surfaces are shown in Fig. 1 as solid lines. These surfaces were fitted to Morse functions with the following parameters: $T_e(X)=0$, $D_0(X)=2900\text{ cm}^{-1}$, $\beta(X)=7.1\text{ \AA}$, $r_e(X)=2.8\text{ \AA}$; $T_e(B)=20\,510$, $D_0(B)=18\,850\text{ cm}^{-1}$, $\beta(B)=3.306\text{ \AA}$, $r_e(B)=3.305\text{ \AA}$. These data provide no information about the attractive part of the B (Franck–Condon) potential, but for computational purposes the nine points obtained from the data (see Fig. 1) were fitted to a Morse potential whose parameters are given above. Since the observed transitions all terminate on the repulsive part of the B -state potential, the results are not sensitive to the shape of this function at large internuclear separations. *These surfaces, particularly that of the B state should be considered very approximate at this time.* The B potential represents a Franck–Condon state corresponding to HgI (B) in the X -state solvent configurations. They predict the spectra of Fig. 5, the wavelength dependence of the beat frequencies and the beat and population amplitudes. The X potential is clearly very similar to that in the gas phase. The frequencies of this new potential are characterized as: $E_{n''}^{(s)}/hc = 127.2(n'' + 1/2) - 1.09(n'' + 1/2)^2$. This paper is concerned with vibrational relaxation in the X state so the B -state surface need only be known approximately in order to obtain the time dependence of the probe absorption coefficient at each probe wavelength. The beat frequencies appear to indicate which level is being probed in the X state. A more detailed account of the oscillatory portions of the signal will be presented in a separate publication.⁴⁴

F. Contact charge transfer complexes of I atoms with solvent molecules

Solvated I atoms are known to form contact charge transfer complexes with polar solvent molecules. These com-

plexes have been spectroscopically characterized⁴⁵ by broad electronic absorption bands in the ultraviolet spectral region. The I atom generated upon photodissociating HgI₂ in ethanol, is expected to complex into an I:ethanol (I:ETOH) species. The peak absorption for I:ETOH is reported to be at 360 nm, so it is possible that this band contaminates the spectral region between 400 and 510 nm, in which the HgI dynamics are reported. Therefore it is important to ascertain the various contributions to the signals presented in Fig. 3. This is accomplished by considering two pieces of information. (1) The contact charge transfer complex of I atoms with a solvent partner possess absorption spectra that are highly solvent sensitive. For example, the species I:H₂O, I:MEOH, I:ETOH, and I:IPROP (isopropanol) yield absorption maxima at 255, 330, 360, and 380 nm, respectively. This spectral shifting is correlated to the solvent ionization potentials which are 12.60, 10.85, 10.50, and 10.15 eV for H₂O, methanol, ethanol and isopropanol, respectively, and the absorption profile for each of the complexes (except I:ETOH) are reported in Ref. 45. (2) A comparison of the oscillatory signal component, assumed to be due to HgI, with the total signal amplitude was made for the three alcohol solvents, at 400 and 440 nm. If I:Solvent were dominating the transient absorption signals, the signal amplitude would increase by a factor of ca. 2.6 at 400 nm, when conducting the photolysis reaction in isopropanol vs methanol. This increase in signal is expected to arise because of the difference between the relative absorption strengths of I:MEOH and I:IPROP.⁴⁵ No interference is expected at 440 nm in methanol since I:MEOH reportedly does not absorb at this wavelength. The molar extinction coefficients for I:MEOH and I:ETOH⁴⁵ at 400 nm are ca. 300 l/(mol*cm) which are approximately a factor of 5 less than ϵ_{max} . The molar extinction coefficient for HgI is estimated to be ca. 800 l/(mol*cm) from calculated and observed Einstein coefficients.⁴⁶ In Fig. 6(a) the result of photolyzing HgI₂ in methanol, ethanol and isopropanol are shown. The earliest time spike involves the dissociation of the HgI₂ parent molecule and is relatively insensitive to the solvent—the parent absorption spectra are nearly identical in all of the solvents. After the molecule has dissociated an HgI wave-packet oscillation is observed. The modulation depth of the oscillation in isopropanol is ca. one-half of that observed in methanol and ethanol, and the overall (mean) signal (at times > 250 fs) is slightly larger for the isopropanol experiment. These data in conjunction with the data of Ref. 45, provide an estimate of the amount of I:Solvent present in our transients.

Assuming the decreased modulation depth in isopropanol is due to the increased absorption strength of the I:IPROP species at 400 nm relative to that of I:MEOH/ETOH it may be concluded that I:MEOH/ETOH accounts for as much as 25% of the total signal. On the other hand, the molar extinction coefficient for I:IPROP at 400 nm is reportedly 2.6 times larger than that for I:MEOH/ETOH⁴⁵ which leads to the conclusion that the contribution of the I:MEOH and I:ETOH complexes to the signals is only ca. 4%. The lower estimate is probably more reliable because the modulation depth of the oscillations also may be solvent sensitive, because factors related to HgI-solvent forces may be in-

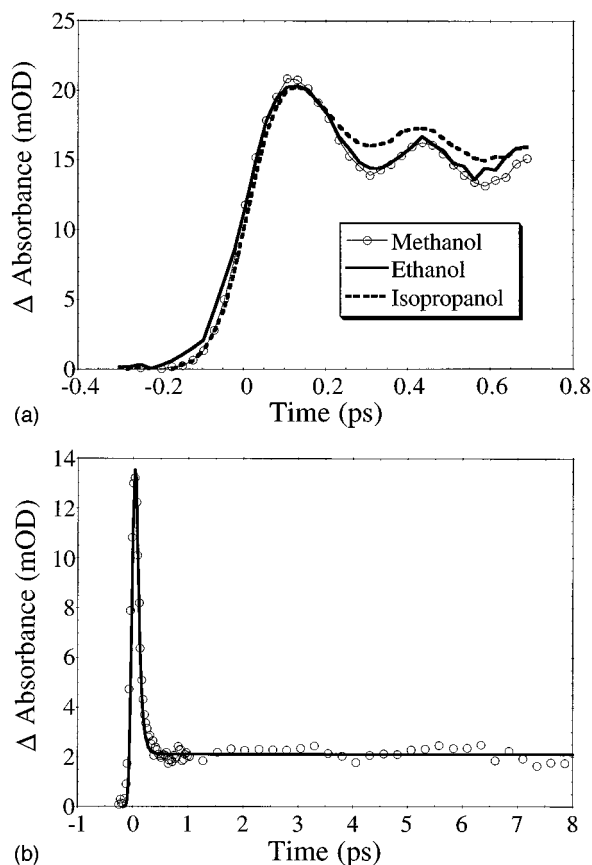


FIG. 6. (a) Pump-probe transients of HgI_2 samples in methanol, ethanol and isopropanol are shown. (b) The transient absorption of a 1 M solution 1-iodoperfluorbutane is shown. The data is fit to a molecular response consisting of a rapidly decaying exponential and a constant background, convoluted with an instrument function. The time constant for the rapid decay fits to a value of 80 fs.

involved in the variation of the beat amplitude with solvent. At 440 nm the signals obtained in ethanol and methanol are identical, so the presence of an I:Solvent complex is even less important at this wavelength.

In order to verify a contribution from I:ETOH and to determine if any transient behavior could be attributed to this species, iodine atoms were directly generated by photolysis of 1-iodoperfluorbutane (IPFB) in ethanol. It is well known that by photolyzing iodoalkanes in the band corresponding to the iodine $n \rightarrow \sigma^*$ transition, the C–I bond cleaves to generate a free iodine atom and an alkyl radical. In Fig. 6(b) the magic angle pump-probe results are shown for a probe wavelength at 420 nm and the same number of absorbed photons as in the HgI_2 experiments. No signal components indicative of fast recombination of I atoms have been detected in either the HgI_2 or the IPFB samples. The quantum yield for photodissociating I atoms for both compounds is therefore estimated to be close unity. The IPFB signal exhibits a large, instantaneous absorption spike that is attributed to a two photon absorption via the (n, σ^*) state. For delays greater than 250 fs, the signal approaches a constant level of ca. 2 mOD which corresponds to ca 10% of the HgI_2 signal. Furthermore, after ca. 250 fs the signal exhibits a vanishingly small anisotropy. The rapid approach of the anisotropy to

zero is indicative of the C–I bond breaking, followed by the formation of contact charge transfer complexes of the iodine atom with a broad distribution of ethanol molecule configurations. The perfluorbutyl radical is not expected to have any electronic absorption in this region. In any event such transitions would show an anisotropy decaying on the timescale of rotational diffusion. Moreover, these data show *no* evidence of dynamics similar to those found for the HgI_2 experiments (see Fig. 3 and 5) at time delays considerably later than 250 fs.

G. Summary of results

The conclusions from this section are now briefly summarized. (1) Vibrational coherence in the product states of HgI are observed following the femtosecond photolysis of HgI_2 . The frequencies of the oscillations vary with probe wavelength indicating transitions are occurring from a slightly perturbed version of the gas phase anharmonic potential. (2) These vibrational frequencies and their associated probe wavelengths fix vertical $B \leftarrow X$ transition frequencies based on X -state quantum numbers. (3) Two independently calculated unrelaxed spectra generated from the fits of the slower signal components and the amplitudes of the oscillations coincide, signalling that vibrationally hot HgI exists at early times. (4) The spectral evolution is indicative of vibrationally hot HgI molecules, cooling to form the long wavelength side of the equilibrated HgI absorption band. (5) A comparison of the signal sizes at 400 nm for different solvents provide an estimate of the I:ETOH contribution to the HgI_2 signals. (6) The photolysis of IPFB produces a transient signal that exhibits no detectable anisotropy after 250 fs, and no noticeable dynamics on the timescale of the signal evolution of Fig. 3. This signal is ≈ 10 times smaller (per absorbed pump photon) than the signal from HgI_2 and indicates that the HgI absorption strength is stronger in solution, relative to the gas phase. (7) Molecular dynamics simulations are consistent with the equilibrated X state being only slightly modified by the solvent.

These results imply that the presented oscillatory behavior and subsequent signal evolution are assigned to arise from vibrationally excited HgI fragments: The former corresponds to wave-packet dynamics and the latter to the slower solvent induced relaxation of the vibrational population, which forms the subject of the remainder of this paper.

IV. VIBRATIONAL RELAXATION DYNAMICS

After the vibrational wave packet is fully dephased by HgI -solvent collisions, any further changes in the signal involve the relaxation dynamics of the pure vibrational population distribution of the HgI photofragments. The initial nonequilibrated vibrational distribution arises from the partitioning of the excess photodissociation energy between the recoiling atomic and diatomic fragments, and the evolving signals correspond to the dynamics of the “hot” distribution as it approaches equilibrium. The difference between each transient is a consequence of the relaxing population sweeping into, and then out of resonance with each of the probe

wavelengths. This becomes evident in a qualitative manner when examining the Morse potentials shown in Fig. 1.

The vibrational relaxation data shown in Fig. 3 are not fully described by a single relaxation rate coefficient or a T_1 time, as would be the case for a harmonic oscillator. A harmonic treatment with linear coupling formally excludes the effects introduced by energy relaxing through multiple quantum jumps ($n \rightarrow n - m$, for $m > 1$). Furthermore, only one frequency component of the solvent power spectrum is used to promote vibrational relaxation in a harmonic potential—namely that at the fundamental frequency of the oscillator. It is clear from the previous section that the system under study is anharmonic. Therefore, anharmonic contributions will be included in the modeling of the data, and as a result a level pair dependence of the relaxation rate naturally evolves. The modeling of the anharmonic HgI oscillator coupled to the solvent vibrational modes will also characterize the average vibrational energy in the oscillator $\langle E_{\text{vib}} \rangle(t)$, and the time evolving electronic spectrum.

The data were modeled by means of a population master equation, in which the state-to-state rates are incorporated. Since state specific vibrational relaxation parameters are not directly measured, the electronic absorption spectrum of HgI also must be reproduced for each ground state population distribution. By considering this relaxation model for the anharmonic oscillator, and calculating the electronic absorption spectrum for an instantaneous population distribution, the time resolved transients may be simulated. The model described below calculates the level dependent population dynamics in the anharmonic ground state of HgI by first choosing an initial population distribution which originates from the 320 nm photolysis of HgI₂. The time dependent population for each vibrational state in the HgI product is described in terms of the coupled diagonal density matrix elements, $\rho_{nn'}(\tau)$. The off-diagonal elements of the product density matrix which are responsible for the observed vibrational coherence, are assumed to have negligible effect on the population dynamics and are therefore excluded from the present analysis.⁴⁷ The calculation of the population flow is formulated in a way that leads to an estimate of the frequency-dependent friction exerted on the solute by the solvent cage, and therefore places the analysis within the context of the current theoretical concepts for vibrational relaxation.

A. Anharmonic oscillator coupled to harmonic bath vibrations

A number of different approaches can be used to model the vibrational relaxation in an anharmonic potential by means of master equations. In the absence of a detailed knowledge of the energy transfer pathways, the only strict requirement for the solutions is that $R_{n \rightarrow n-m}$, the state-to-state rate coefficient for transitions between quantum states $|n\rangle$ and $|n-m\rangle$, is related to $R_{n-m \rightarrow n}$ through detailed balance:

$$R_{n-m \rightarrow n} = e^{-\beta E_{n,n-m}} R_{n \rightarrow n-m}. \quad (6)$$

The first approach used here is to suppose that the HgI and

the solvent motions are quantum mechanical and that the coupling of the HgI to the solvent is linear in both the HgI stretching coordinate and the solvent coordinates. Furthermore, the relevant solvent motions are considered to be harmonic. This is a common assumption in solid-state relaxation theory^{1,4} which naturally leads to spontaneous decay and solvent induced processes analogous to well-known properties of photons coupling to a two level system.⁴⁸ The spontaneous part corresponds to the generation of phonons (solvent motions) from solute vibrational excitations and the induced part consists of the temperature-dependent removal or creation of phonons accompanying the deexcitation or excitation of solute motions. The boson occupation number, \bar{n}

$$\bar{n}(\omega_{nn'}) = 1 / (\exp(\hbar \omega_{nn'} / k_B T) - 1) \quad (7)$$

evaluated at the solute transition frequency $\omega_{nn'}$ for vibrational states n and n' , limits the rate of induced transitions. For a spontaneous rate coefficient γ the rate constant for upward transitions is $\bar{n}(\omega_{nn'}) \gamma$ and for downward transitions it is $(\bar{n}(\omega_{nn'}) + 1) \gamma$. This approach will be compared with one using a collisional master equation.

1. Vibrational master equation approach

The population master equation for the relaxation of the n th level in an anharmonic potential with N levels, coupled bilinearly to a harmonic bath is therefore proposed to have the form,

$$\begin{aligned} \dot{\rho}_n(t) = & - \left\{ \sum_{m=1}^n \gamma_{n,n-m} [\bar{n}(\omega_{n,n-m}) + 1] \right. \\ & + \left. \sum_{m=1}^{N-n} \gamma_{n+m,n} [\bar{n}(\omega_{n+m,n})] \right\} \rho_n(t) \\ & + \sum_{m=1}^{N-n} \gamma_{n+m,n} [\bar{n}(\omega_{n+m,n}) + 1] \rho_{n+m}(t) \\ & + \sum_{m=1}^n \gamma_{n,n-m} [\bar{n}(\omega_{n,n-m})] \rho_{n-m}(t). \end{aligned} \quad (8)$$

The factors, $\gamma_{n,n'}$ are the spontaneous (quantum mechanical) state-to-state rate coefficients for each of the designated two-level systems. If the vibrational relaxation rate of the solute is fast compared with the thermal diffusion of the solvent $\bar{n}(\omega)$ would exhibit a time dependence. In this analysis the occupation number of the solvent is treated as a time-independent quantity. Thermal dissociation to the Hg+I continuum is not included in the model, and this leads to only downward transitions when $n = N$. In the present analysis the rate coefficients are defined as

$$\gamma_{n,n'} = |r_{n,n'}|^2 G(\omega_{n,n'}). \quad (9)$$

The reduced matrix elements $r_{nn'} = (\mu \omega_{n,n'} / \hbar)^{1/2} \langle n | r | n' \rangle$ (μ is the reduced mass of the diatomic) are dimensionless and $G(\omega_{n,n'})$ is a frequency-dependent, temperature-independent rate which will be determined by fitting the ex-

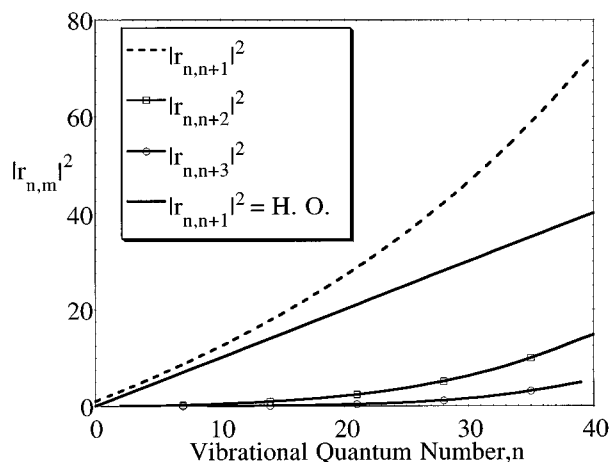


FIG. 7. Characterization of the off diagonal matrix elements which linearly couple the anharmonic HgI oscillator to the harmonic solvent. For comparison, the nonzero matrix elements are also shown as a linear function of n for the harmonic oscillator (H.O.).

perimental data to Eqs. (8) and (5). We have not found an analytic solution using Eq. (8) for the energy relaxation of an anharmonic oscillator in a bath of harmonic oscillators. The energy decay will generally be nonexponential, different from the exponential decay of the harmonic oscillator energy.¹⁴

Equation (8) seems reasonable because it is an empirical extension to an anharmonic oscillator of the well-known harmonic model, made possible by incorporating the $\gamma_{n,n'}$ associated with all level pairs, rather than just adjacent ones. In this situation, Eqs. (7)–(9) lead to a relaxation matrix that is not tridiagonal as in the harmonic case. Figure 7 shows the nonlinearity of the relation between $|r_{n,n'}|^2$ and n for the HgI oscillator. The n dependence of $|r_{n,n+m}|^2$ for values of $m=1, 2$, and 3 are shown in this figure. The data of Fig. 7 imply that for an oscillator having an anharmonicity of approximately 1% of the fundamental frequency, only the matrix elements which are off diagonal by <3 contribute to the vibrational relaxation dynamics. Couplings with $\Delta n > 3$ become significant only near the top of the well.

2. The collisional master equation approach

A collisional master equation, different from Eq. (8) but that also satisfies detailed balance, is commonly used to model collisionally induced vibrational relaxation in the gas phase. This approach would certainly be a valid mechanism if the primary mode of energy disposal involved the coupling to translational degrees of freedom of the surrounding bath.⁴⁹ Such a master equation has been previously used in the harmonic limit to model vibrational relaxation of solutes in liquids,^{7–9} and is therefore presented to compare with Eq. (8). In an analogous manner to Eq. (8), the collisional master equation for an anharmonic oscillator is proposed to have the form

$$\begin{aligned} \dot{\rho}_n(t) = & - \left\{ \sum_{m=1}^n \gamma_{n,n-m} + \sum_{m=1}^{N-n} \gamma_{n+m,n} \right. \\ & \times \exp\left(-\frac{\hbar\omega_{n+m,n}}{k_B T}\right) \left. \right\} \rho_n(t) \\ & + \sum_{m=1}^{N-n} \gamma_{n+m,n} \rho_{n+m}(t) \\ & + \sum_{m=1}^n \gamma_{n,n-m} \exp\left(-\frac{\hbar\omega_{n,n-m}}{k_B T}\right) \rho_{n-m}(t). \quad (10) \end{aligned}$$

In Eq. (10) the $\gamma_{n,n'}$ are identical to those defined in Eq. (9). The primary difference between Eq. (8) and (10) is found in the temperature dependence. In the collisional master equation the temperature dependence comes in the form of Boltzmann factors which are different for each level pair, and the relaxation mechanism does not consider downward transitions stimulated by the excitations present in the bath. The results lead to a characteristic timescale that is approximately twice as fast as that obtained from Eq. (8) for a fixed matrix of $\gamma_{n,n'}$.

B. Simulation of transients

The functions of Fig. 2 can be used to estimate the initial population of the HgI fragment after photolysis, $\rho(0)$, by examining the time dependence of a signal for a particular probe wavelength. For example, if the initial population was centered at $n''=35$, the 490 nm transient would rise as the n'' states near $n''=27$ were populated from above. As the population relaxed further into the $n''=15$ – 20 region, the signal would exhibit a decay corresponding to the decrease in occupation of the portion of the manifold absorbing at this wavelength. A subsequent growth and decay of the molecular response would be present as the population relaxed into the lowest region of the manifold. This feature would arise because of the second maximum in the spectral function centered near $n''=8$ for this probe wavelength. This type of signal variation is indicative of the initial population in the HgI fragment, and provides the basis for the choice of $\rho(0)$ (see below).

The rate of population relaxation for a given level pair in HgI is defined in Eq. (9). The matrix elements $|r_{n,n'}|^2$ were determined through the analysis of the X potential surface of solvated HgI. Thus, calculating each rate coefficient $\gamma_{n,n'}$, depends on the form of $G(\omega_{n,n'})$, which is not known *a priori*. In this simulation, the *shape* of the vibrational contribution to the power spectrum of neat ethanol was utilized as a first attempt for $G(\omega_{n,n'})$. The spectrum, shown in Fig. 8, rises from zero at zero frequency to a peak at ca. 40 cm^{-1} , from which it decays exponentially with increasing ω . At higher frequency, resonances associated with intramolecular motions of ethanol are present, however the range of energies relevant to HgI relaxation (including all of the significant multiple quantum jumps) is from ca. 70 – 250 cm^{-1} , so these features were not necessary to include. The spectrum of Fig. 8 is similar to that reported by Cho *et al.*⁵⁰ and was provided to us by Vöhringer and Scherer.⁵¹ It will serve as a

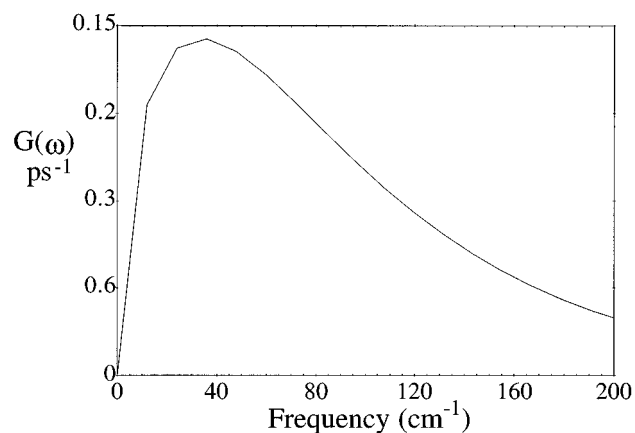


FIG. 8. The vibrational part of the normalized power spectrum of ethanol (see Ref. 50–51). The numerical values of $G(\omega)$ correspond to those that reproduce the HgI data.

model for the relative state density of the harmonic bath of solvent molecules, to which excess vibrational energy from HgI will flow. In principle, the spectrum of $G(\omega)$ could be nonuniformly adjusted to provide the best fits to the observations, however initially the magnitude of the unadjusted power spectrum, which is a relaxation rate in the present units [see Eq. (9)] was found to fit the data reasonably well. This scaled function $G(\omega)$ can be used with Eq. (9) to determine the spontaneous rate coefficient for each level pair. (See note added in proof.)

V. DISCUSSION

The modeling of the relaxation dynamics with Eq. (8) was accomplished by choosing a $\rho(0)$ and by scaling the magnitude of the power spectrum to reproduce the timescales observed for the transients. The results of the simulation are overlaid atop each transient and are shown in Fig. 9. The scaling factor for the power spectrum, was adjusted throughout a range of 0.14–1.0 ps⁻¹. A scaling factor of 0.33 ps⁻¹ and a $\rho(0)$ centered at $n''=9$ with a Gaussian width of 1000 cm⁻¹ were used to generate the curves in Fig. 9. With the exception of the 510 nm transient which shows a slow rise component, the simulations reproduce the observed vibrational relaxation dynamics fairly well at delay times >1 ps. For comparative purposes, simulations for scaling factors of 0.5 and 0.25 ps⁻¹ are also plotted in Fig. 9. This is to show that with a scaling factor other than 0.33 ps⁻¹, the overall population relaxation is either too fast (2 ps) or too slow (4 ps). The data are not complete enough to justify a least-squares fit.

The initial distribution centered near $n''=9$ corresponds to a mean excess energy of ca. 1050 cm⁻¹. The center of this distribution is consistent with the time dependence of the transients as discussed above, however, the fits are not so sensitive to the width of the distribution. The value of 1000 cm⁻¹ was used because this was needed to provide the best fit of the early time spectra shown in Fig. 5. A width of 500 cm⁻¹ generates too narrow a spectrum. It is important to relate this value of $\rho(0)$ to the results of the gas phase dissociation dynamics. The gas phase dissociation of HgI₂ at 320

nm produces the I atom in its $^2P_{3/2}$ and $^2P_{1/2}$ with a 5:1 ratio.²¹ The reaction pathway which produces the $^2P_{3/2}$ ground state I atom, partitions the majority of the excess pump energy into the HgI fragment, producing a vibrationally hot molecule. For the $^2P_{1/2}$ excited state I channel, whose surface lies 7600 cm⁻¹ (corresponding to the spin-orbit splitting of I) above that of the $^2P_{3/2}$ surface, a cold HgI molecule results because the majority of the excess pump energy is used to access the excited state. A similar situation appears to be applicable to the solution phase reaction, with the dominant reaction pathway corresponding to the $^2P_{3/2}$ I channel, resulting in vibrationally hot HgI. Since this channel is favored by a factor of 5 in the gas phase it is not surprising that it also determines the main portion of the initial population distribution in solution as well. The inclusion of a cold HgI distribution (centered at $n''=4$) that was five times smaller than the hot distribution did not alter the calculated results by enough to be significant when compared with the measurements. Therefore, the excited state I channel has been excluded from the present simulation.

The applicability of the master equation used here depends on the mechanism for vibrational energy transfer from HgI into the solvent. It has been assumed that this process is dominated by the coupling of the quantum vibrations in the solute to a bath of harmonic quantum oscillators. This is an assumption which seems plausible when considering that we are dealing with a structured solvent in which a significant density of low-frequency librational and torsional modes is expected to be present throughout the energy range of the contributing HgI level pairs. However, it must be emphasized that the only requirement for a legitimate set of rate equations is that detailed balance be upheld. The physics of the system will then govern the specifics of the master equation required. With this in mind the collisional master equation was also used to model the HgI relaxation. This approach implies that the energy disposal mechanism involves changes in solvent momentum during collisions with the hot solute. Thus, a situation similar to vibrational–translational (V–T) energy transfer would prevail instead of vibrational–vibrational (V–V) transfer. This treatment could also model the relaxation data if the scaling factor rate is increased by a factor of 2. For the case of vibrational energy high in the well, where the energy separation between level pairs becomes small compared with the possible harmonic frequencies of the liquid, the collisional master equation may better characterize the relaxation dynamics. A better approach than either the harmonic bath or the collisional master equation might be to incorporate both by writing $G(\omega)$ as $H(\omega) + C(\omega)$, in which H represents the contribution of (harmonic) vibrations of the solvent and C represents the contribution from other motions. Replacing the $G(\omega)$ implicit in Eq. (8) for $\dot{\rho}_n^{(H)}(t)$ by $H(\omega)$ and that implicit in Eq. (10) for $\dot{\rho}_n^{(C)}(t)$ by $C(\omega)$, the total population dynamics could be obtained from $\dot{\rho}_n(t) = \dot{\rho}_n^{(H)}(t) + \dot{\rho}_n^{(C)}(t)$. In this way the dynamics are determined by $V \rightarrow V$ transfer when $H(\omega) \gg C(\omega)$ and by $V \rightarrow T$ or $V \rightarrow R$ transfer when $H(\omega) \ll C(\omega)$. At present, neither is the apportionment of the spectrum of solute–solvent forces into H and C components known for ethanol, nor is our data extensive enough to merit such a fitting pro-

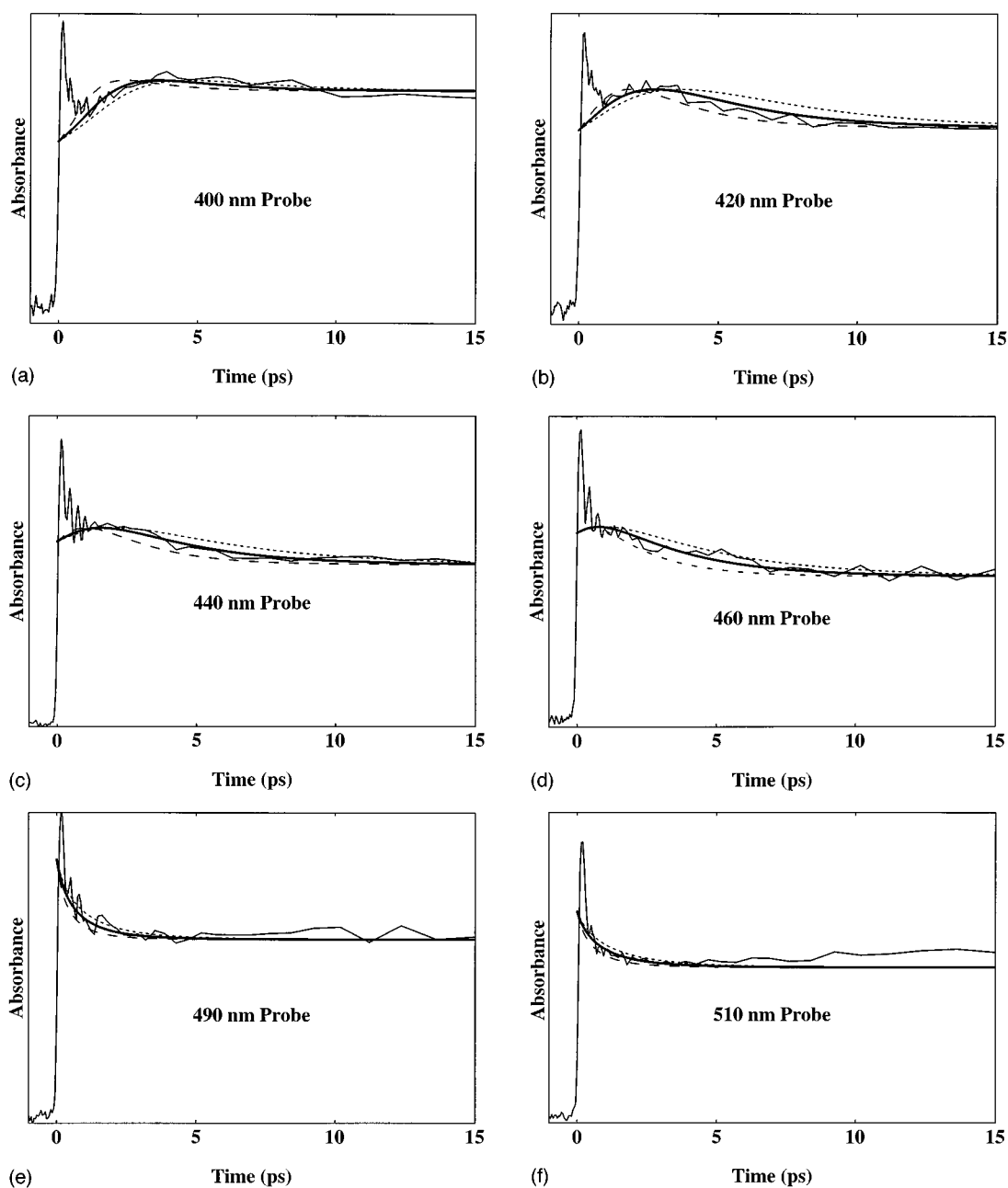


FIG. 9. Simulation of the wavelength dependence of the population dynamics. The long dashed line represents a simulation for $\gamma_{10}=0.5 \text{ ps}^{-1}$, the solid line for $\gamma_{10}=0.33 \text{ ps}^{-1}$ and the short dashed line is for a value of $\gamma_{10}=0.25 \text{ ps}^{-1}$.

cedure. It should also be noted, that the two master equations contain different temperature dependencies. Therefore, the study of vibrational relaxation with respect to temperature could provide distinctions between the two approaches. It is also not clear why the power spectrum of the solvent is adequate to model the spectrum of the forces relevant to vibrational relaxation. Presumably the shape of the spectrum of the forces would not coincide with the power spectrum over a wider frequency range. It will be useful to use the molecular dynamics simulations to examine this point. (See note below.)

When the value of $G(\omega_{0,1})=0.33 \text{ ps}^{-1}$ [obtained from simulating the data with Eq. (8)] is multiplied by $|r_{0,1}|^2$ as defined in Eq. (9), a state-to-state relaxation time of 2.9 ps

for the $n''=1 \rightarrow 0$ transition is obtained. This relaxation time was 1.5 ps when the collisional master equation was employed. For the remaining discussion only the results obtained from Eq. (8) will be considered. Equation (9) then automatically yields the state-to-state rate constants associated with the relaxation of each level pair. The quantities $|r_{n,n'}|^2$ and $G(\omega_{n,n'})$ can be determined from Figs. 7 and 8, respectively, and $\omega_{n,n'}$ can be evaluated by utilizing the X surface given in Sec. III E. The state-to-state rate associated with the $n''=15 \rightarrow 14$ is calculated to be 8.94 ps^{-1} . Other values are $\gamma_{15,13}=0.146 \text{ ps}^{-1}$ and $\gamma_{15,12}=0.002 \text{ ps}^{-1}$. This implies that $n''=15$ transfers population downward to $n''=14$, 13, and 12 with time constants of $0.11(\bar{n}(\omega_{15,14})+1)$, $6.8(\bar{n}(\omega_{15,13})+1)$, and $408(\bar{n}(\omega_{15,12})+1)$ ps, respectively. Of

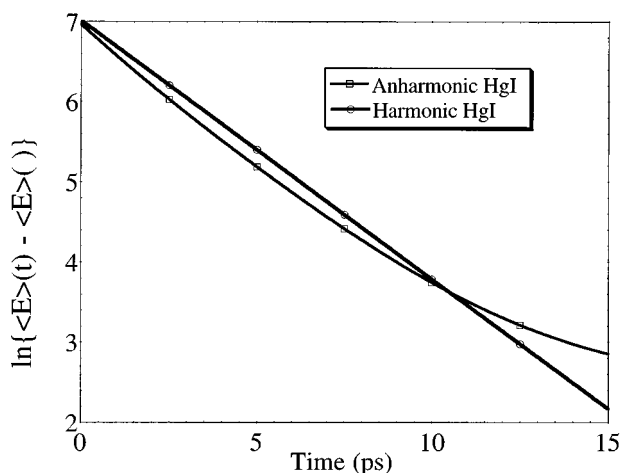


FIG. 10. The natural logarithm of the excess energy in HgI is plotted with respect to time. The result for a harmonic oscillator having a fundamental frequency of 125 cm^{-1} is also shown with $\gamma_{10}=0.33\text{ ps}^{-1}$.

course the *total* energy relaxation out of this region of the potential surface also depends on the upward transitions which scale as $\bar{n}(\omega_{n,n'})$ in the model described by Eq. (8). When summing over all of the possible state-to-state rates, the decay of the total energy in excess of equilibrium in the anharmonic well is expected to be nonexponential. This is demonstrated in Fig. 10 in which a logarithmic plot of the total energy in the oscillator as a function of time is shown for the simulated results. This should be contrasted with the harmonic oscillator result in which the decay of the total energy would exhibit an exponential behavior with a time constant T_1 . The harmonic energy decay is also shown for an oscillator having a 125 cm^{-1} frequency and a T_1 value of 3 ps. Our analysis shows that the differences between a model using frequency-dependent rates (and all multiple quantum jumps) and a harmonic oscillator model are significant only near the top of the well. Efforts are underway to create a more energetic product fragment to more fully examine the new exponential character of the energy relaxation higher in the anharmonic well.

High in the potential well, the fast population relaxation discussed above will also have implications for the loss of coherence associated with these level pairs. The total vibrational dephasing rates contain both pure dephasing and population relaxation. If the population relaxation becomes the dominant dephasing mechanism, problems will arise with the standard approaches to vibrational relaxation.^{3,52} If a wave packet possesses a narrow distribution of discrete position eigenstates, and if population relaxation occurs on a timescale that is faster than the vibrational period, the relaxation rate should depend on the location of the wave packet in the well. It follows that theoretical approaches in which the solute-solvent coupling is expanded to first order in the equilibrium internuclear separation,⁵² may omit some of the essential physics of the relaxation. Under these circumstances the molecule cannot exercise the full amplitude of its vibrational motion on the timescale of population relaxation, so a specific force-force autocorrelation function probably

would need to be defined at each relevant position along the vibrational coordinate while the wave packet was intact. It may be better to work in a position basis set in this limit. Such fast relaxation also points to the necessity of incorporating coherences into the master equations. Certainly the early time dynamics near the top of the well should incorporate a master equation with both relaxation of coherences and populations as well as their interchanges such as would be obtained from conventional second-order relaxation theory.⁵³ This approach will be used in another publication in which it is experimentally verified that the coherence high in the well is retained by population dynamics.⁴⁴

Another aspect of the relaxation dynamics relates to the fact that the magnitude of the dipole moment in HgI varies with internuclear separation. Its value at the equilibrium distance is ca. 2 D. At large internuclear separations the dipole moment approaches zero as the molecule dissociates to mercury and iodine atoms. High in the well, such as for the initial condition of $n''=9$, the molecule will therefore experience a variation in its interaction with the solvent as it samples the repulsive and attractive sides of the potential surface. If this occurs during the motion of the wave packet, then different relaxation rates would be observed on the attractive and repulsive parts of the potential surface where the HgI dipole interactions with the solvent vary.

The timescales for vibrational relaxation determined by these experiments is comparable with those observed for molecular ions in polar solutions,⁵⁴ for which the solute-solvent force along the solute normal coordinate is in fact very large. The absence of a net charge on this system seems to be countered by its significant dipole moment of ≈ 2 D. The dependence of the magnitude of this dipole on the internuclear separation is analogous to the charge switching problem in I_2^- which has recently been shown to be important in understanding its relaxation dynamics.⁵⁵

VI. CONCLUSION

Master equations were utilized to determine characteristic timescales which reproduce the experimental data for the vibrational relaxation of HgI following the dissociation of HgI₂. The anharmonicity of the HgI solute and a density of solvent states described by the power spectrum of neat ethanol were fully included to describe the vibrational population dynamics. The first master equation discussed was based on the assumption that the solute transfers its energy via $V \rightarrow V$ coupling with the solvent modes. This amounted to a relaxation time for the $n''=1 \rightarrow 0$ transition of 2.9 ps. A collision model was also tested and this yielded timescales which were faster by a factor of 2 (ca. 1.5 ps). The two values might provide a lower and upper limit of the true solution phase population relaxation dynamics. All of the state-to-state relaxation rates for the HgI ground state are calculable through the model. The influence of anharmonicity is presented as a necessary mechanism for energy disposal in the well. The influence of the anharmonicity on the energy relaxation was illustrated by the nonexponential decay of the total energy out of the HgI system. The simulations of the data also resulted in an estimate for the initial

excess energy of the HgI which was centered near $n''=9$. This corresponds to a total excess energy of ca. 1047 cm^{-1} . The fast timescales of vibrational relaxation are comparable to vibrational relaxation dynamics for molecular ions in polar solutions, indicating that the forces on the vibrational coordinate are large. Although the vibrational coherence will be quantitatively analyzed in a later publication,⁴⁴ HgI was shown to be formed in a coherent superposition state which dephases with a time constant of ≤ 1 ps depending on which part of the well is probed.

Note added in proof. We recently determined the force–force autocorrelation function and its spectrum for HgI in ethanol using molecular dynamics simulations.⁵⁶ The results show that power spectrum of Fig. 8 in the region $70\text{--}130\text{ cm}^{-1}$ is virtually identical with the spectrum of relevant forces thereby justifying the procedure used in the text for these low frequencies. The value of T_1 calculated from the simulation is 2 ps, in rather good agreement with the experimental value. The fluctuations in the Lennard-Jones forces appear to be mainly responsible for relaxation while the charges determine the structure of the solvent–solute complex.

ACKNOWLEDGMENTS

This work was supported by NSF-CHE and NIH. N.P. gratefully acknowledges the National Science Foundation for a postdoctoral fellowship in chemistry.

¹F. Legay, in *Chemical and Biological Applications of Lasers*, edited by C. B. Moore (Academic, New York, 1977), Vol. II.
²J. Chesnoy and G. M. Gale, *Adv. Chem. Phys.* **70**, 297 (1988).
³J. Owrutsky, D. Raftery, and R. M. Hochstrasser, *Annu. Rev. Phys. Chem.* **45**, 519 (1994).
⁴I. Oppenheim, K. E. Schuler, and G. H. Weiss, *Stochastic Processes in Chemical Physics: The Master Equation* (MIT, Cambridge, MA, 1977).
⁵A. Seilmeier and W. Kaiser, in *Topics in Applied Physics; Ultrashort Laser Pulses-Generation and Applications*, edited by W. Kaiser (Springer-Verlag, New York, 1992), Vol. 60.
⁶E. J. Heilweil, M. P. Casassa, R. R. Cavanagh, and J. C. Stephenson, *Annu. Rev. Phys. Chem.* **40**, 143 (1989).
⁷A. L. Harris, J. K. Brown, and C. B. Harris, *Annu. Rev. Phys. Chem.* **39**, 341 (1988), and references therein.
⁸U. Banin and S. Ruhman, *J. Chem. Phys.* **98**, 4391 (1993); I. Benjamin, U. Banin, and S. Ruhman, *ibid.* **98**, 8337 (1993); U. Banin, R. Kosloff, and S. Ruhman, *Chem. Phys.* **183**, 289 (1994).
⁹D. A. V. Kliner, J. C. Alfano, and P. F. Barbara, *J. Chem. Phys.* **98**, 5375 (1993); J. C. Alfano, Y. Kimura, P. K. Walhout, and P. F. Barbara, *Chem. Phys.* **175**, 147 (1993).
¹⁰N. Pugliano, D. K. Palit, A. Z. Szarka, and R. M. Hochstrasser, *J. Chem. Phys.* **99**, 7273 (1993).
¹¹R. M. Whitnell, K. R. Wilson, and J. T. Hynes, *J. Chem. Phys.* **96**, 5354 (1992); *J. Phys. Chem.* **94**, 8625 (1990).
¹²M. Bruehl and J. T. Hynes, *Chem. Phys.* **175**, 205 (1993).
¹³I. Benjamin and R. M. Whitnell, *Chem. Phys. Lett.* **204**, 45 (1993).
¹⁴M. Tuckerman and B. J. Berne, *J. Chem. Phys.* **98**, 7301 (1993); J. S. Bader and B. J. Berne, *ibid.* **100**, 8359 (1994).
¹⁵F. E. Figueirido and R. M. Levy, *J. Chem. Phys.* **97**, 703 (1992).
¹⁶J. T. Yardley, *Introduction to Molecular Energy Transfer* (Academic, New York, 1980).
¹⁷J. C. Polanyi, *Appl. Opt. Suppl.* **2**, 109 (1965); J. V. V. Kasper and G. C. Pimentel, *Phys. Rev. Lett.* **14**, 352 (1965).
¹⁸N. Pugliano, A. Z. Szarka, D. K. Palit, and R. M. Hochstrasser, *Ultrafast Phenomena IX*, edited by G. Mourou, A. H. Zewail, P. F. Barbara, and W. H. Knox, Springer Series Chem. Phys. **60**, 501 (1994).
¹⁹N. Pugliano, D. Raftery, E. Gooding, A. Szarka, and R. M. Hochstrasser, *Ultrafast Phenomena IX*, edited by G. Mourou, A. H. Zewail P. F. Barbara,

and W. H. Knox, Springer Series Chem. Phys. **60**, 63 (1994).
²⁰J. Maya, *IEEE J. Quan. Electron.* **QE-15**, 579 (1979).
²¹H. Hoffmann and S. R. Leone, *J. Chem. Phys.* **69**, 3819 (1978).
²²A. Loewenschuss, A. Ron, and O. Schnepp, *J. Chem. Phys.* **50**, 2502 (1969); M. Wehrli, *Helv. Phys. Acta.* **13**, 153 (1940).
²³T. R. Griffiths and R. A. Anderson, *J. Chem. Soc., Faraday Trans. II* **75**, 957 (1979).
²⁴K. J. Jordan, H. A. Bascal, R. H. Lipson, and M. Melchoir, *J. Mol. Spectrosc.* **159**, 144 (1993); K. J. Lipson, R. H. Lipson, and D. S. Yang, *J. Chem. Phys.* **97**, 9099 (1992); K. J. Jordan, R. H. Lipson, N. A. McDonald, and R. J. LeRoy, *J. Phys. Chem.* **96**, 4778 (1992).
²⁵F. M. Zhang, D. Oba, and D. W. Setser, *J. Phys. Chem.* **91**, 1099 (1987); T. D. Dreiling and D. W. Setser, *J. Chem. Phys.* **79**, 5423 (1983).
²⁶K. S. Viswanathan and J. Tellinghuisen, *J. Mol. Spectrosc.* **98**, 185 (1983).
²⁷J. A. McGarvey, N. Cheung, A. C. Erlandson, and T. A. Cool, *J. Chem. Phys.* **74**, 5133 (1981); N. Cheung and T. A. Cool, *J. Quant. Spectrosc. Radiat. Transfer* **21**, 397 (1979).
²⁸W. R. Wadt, *Appl. Phys. Lett.* **34**, 658 (1979).
²⁹R. M. Bowman, M. Dantus, and A. H. Zewail, *Chem. Phys. Lett.* **156**, 131 (1989); M. Dantus, R. M. Bowman, M. Gruebele, and A. H. Zewail, *J. Chem. Phys.* **91**, 7437 (1989).
³⁰M. Gruebele, G. Roberts, and A. H. Zewail, *Phil. Trans. R. Soc. London, Ser. A* **332**, 223 (1990).
³¹T. Baumert, S. Pedersen, and A. H. Zewail, *J. Phys. Chem.* **97**, 12 447 (1993).
³²S. Pedersen, T. Baumert, and A. H. Zewail, *J. Phys. Chem.* **97**, 12 460 (1993).
³³It should be noted that in Ref. 10 the center frequency of the fundamental was 660 nm.
³⁴J. Maya, *J. Chem. Phys.* **67**, 4976 (1977).
³⁵R. J. Leroy, Program Manual for LEVEL 5.2; University of Waterloo, Chemical Physics Research Report CP-330 (1993).
³⁶R. J. Sension and H. L. Strauss, *J. Chem. Phys.* **88**, 2289 (1988).
³⁷B. R. Brooks, R. E. Bruccoleri, B. D. Olafson, D. J. States, S. Swaminathan, and M. Karplus, *J. Comp. Chem.* **4**, 187 (1983).
³⁸P. J. Hay and W. R. Wadt, *J. Chem. Phys.* **82**, 270 (1985).
³⁹W. R. Wadt and P. J. Hay, *J. Chem. Phys.* **82**, 284 (1985).
⁴⁰P. J. Hay and W. R. Wadt, *J. Chem. Phys.* **82**, 299 (1985).
⁴¹M. J. Frisch, G. W. Trucks, M. Head-Gordon, P. M. W. Gill, D. J. Defrees, J. Baker, J. J. P. Stewart, and J. A. Pople, GAUSSIAN 92 (Gaussian Inc., Pittsburgh, PA, 1992).
⁴²M. P. Allen and D. J. Tildesley, *Computer Simulation of Liquids* (Clarendon, Oxford, 1987).
⁴³(a) B. Dick and R. M. Hochstrasser, *J. Chem. Phys.* **81**, 2897 (1984); B. Dick, R. M. Hochstrasser, and H. P. Trommsdorff, *Nonlinear Optical Properties of Organic Molecules in Crystals, II*, 159 (ATT Bell Laboratories Inc., 1987); (b) Y. J. Yan and S. Mukamel, *Phys. Rev. A* **41**, 6485 (1990).
⁴⁴N. Pugliano, A. Z. Szarka, and R. M. Hochstrasser, in preparation.
⁴⁵P. Fournier de Violet, R. Bonneau and J. Jousot-Dubien, *Chem. Phys. Lett.* **19**, 251 (1973). P. Fournier de Violet, *Rev. Chem. Intermediates* **4**, 121 (1981).
⁴⁶M. F. Mahmood, *J. Phys. D Appl. Phys.* **23**, 1019 (1990); A. Michael and V. Kushawaha, *Spectrosc. Lett.* **23**, 1125 (1990).
⁴⁷In treating the coherence dynamics, as will be done in a future publication (Ref. 44), it is of course necessary to incorporate transfer between coherence and between population elements of the density matrix as is clearly prescribed by Redfield theory (Ref. 44). However in the present case the net amount of coherence is small and can be neglected for times in excess of 1 ps. The density matrix initiating the signal need not be assumed to be diagonal as in Eq. (2), nor is it necessary to assume that $\rho(t)$ is slowly varying as done in the present work.
⁴⁸C. Cohen-Tannoudji, J. Dupont-Roc, and G. Grynberg, *Atom Photon Interactions* (Wiley Interscience, New York, 1992).
⁴⁹E. W. Montroll and K. E. Schuler, *J. Chem. Phys.* **26**, 454 (1957).
⁵⁰M. H. Cho, M. Du, N. F. Scherer, G. R. Fleming, and S. Mukamel, *J. Chem. Phys.* **99**, 2410 (1993).
⁵¹P. Vöhringer, D. C. Arnett, R. A. Westervelt *et al.*, *J. Chem. Phys.* **102**, 4027 (1995).
⁵²D. W. Oxtoby, *Annu. Rev. Phys. Chem.* **32**, 77 (1981); D. W. Oxtoby, *Adv. Chem. Phys.* **47**, 487 (1981).
⁵³A. G. Redfield, *IBM J. Res. Dev.* **1**, 19 (1957); C. P. Slichter, *Principles of*

- Magnetic Resonance* (Springer, Berlin, 1990); C. Cohen-Tannoudji, J. Dupont-Roc, and G. Grynberg, in *Atom-Photon Interactions: Basic Processes and Applications* (Wiley, New York, 1992).
- ⁵⁴M. Li, J. Owrutsky, M. Sarisky, J. P. Culver, A. Yodh, and R. M. Hochstrasser, *J. Chem. Phys.* **98**, 5499 (1993); J. C. Owrutsky, Y. R. Kim, M. Li, M. J. Sarisky, and R. M. Hochstrasser, *Chem. Phys. Lett.* **184**, 368 (1991).
- ⁵⁵B. J. Gertner, K. Ando, R. Bianco, and J. T. Hynes, *Chem. Phys.* **183**, 309 (1994).
- ⁵⁶S. Gnanakaran and R. M. Hochstrasser (unpublished).